Journal for ImmunoTherapy of Cancer

Characterization of intratumoral tertiary lymphoid structures in pancreatic ductal adenocarcinoma: cellular properties and prognostic significance

Xuan Zou,[1,2,3,4] Xuan Lin,[1,2,3,4] He Cheng,[1,2,3,4] Yusheng Chen,[1,2,3,4] Ruijie Wang,[1,2,3,4] Mingjian Ma,[1,2,3,4] Yu Liu,[1,2,3,4] Zhengjie Dai,[1,2,3,4] Yesboli Tasiheng,[1,2,3,4] Yu Yan,[1,2,3,4] Qinqin Hou,[5] Fei Ding,[5] Huan Chen,[5] Xianjun Yu ,[1,2,3,4] Xu Wang ,[1,2,3,4,6] Chen Liu[1,2,3,4]

To cite: Zou X, Lin X, Cheng H, *et al*. Characterization of intratumoral tertiary lymphoid structures in pancreatic ductal adenocarcinoma: cellular properties and prognostic significance. *Journal for ImmunoTherapy of Cancer* 2023;**11**:e006698. doi:10.1136/jitc-2023-006698

► Additional supplemental material is published online only. To view, please visit the journal online (http://dx.doi.org/10.1136/jitc-2023-006698).

XZ, XL, HC and YC contributed equally.

Accepted 09 May 2023

For numbered affiliations see end of article.

Correspondence to
Dr Chen Liu;
liuchen@fudanpci.org

Professor Xu Wang;
wangxu2013@fudan.edu.cn

Professor Xianjun Yu;
yuxianjun@fudanpci.org

ABSTRACT

Background Tumor-associated tertiary lymphoid structures (TLSs) are functional immune-responsive niches that are not fully understood in pancreatic ductal adenocarcinoma (PDAC).

Methods Fluorescent multiplex immunohistochemistry was performed on sequential sections of surgically resected tumor tissues from 380 PDAC patients without preoperative treatment (surgery alone (SA)) and 136 patients pretreated with neoadjuvant treatment (NAT). Multispectral images were processed via machine learning and image processing platforms, inForm V.2.4 and HALO V.3.2; TLS regions were segmented, and the cells were identified and quantified. The cellular composition and immunological properties of TLSs and their adjacent tissues in PDAC were scored and compared, and their association with prognosis was further examined.

Results Intratumoral TLSs were identified in 21.1% (80/380) of patients in the SA group and 15.4% (21/136) of patients in the NAT group. In the SA group, the presence of intratumoral TLSs was significantly associated with improved overall survival (OS) and progression-free survival. The existence of intratumoral TLSs was correlated with elevated levels of infiltrating CD8+T, CD4+T, B cells and activated immune cells in adjacent tissues. A nomogram model was generated with TLS presence as a variable, which successfully predicted PDAC patient OS in an external validation cohort (n=123). In the NAT group, samples exhibited a lower proportion of B cells and a higher proportion of regulatory T cells within intratumoral TLSs. Additionally, these TLSs were smaller in size, with a lower overall maturation level and reduced immune cell activation, and the prognostic value of TLS presence was insignificant in the NAT cohort.

Conclusion Our study systematically revealed the cellular properties and prognostic values of intratumoral TLSs in PDAC and described the potential impact of NAT on TLS development and function.

WHAT IS ALREADY KNOWN ON THIS TOPIC

⇒ The cancer-associated tertiary lymphoid structures (TLSs) are functional immune-responsive niches present in multiple cancer types, but their exact role and context-dependent prognostic value in pancreatic ductal adenocarcinoma (PDAC) are unclear.

WHAT THIS STUDY ADDS

⇒ The study demonstrated the prognostic significance, spatial structures and cellular properties of intratumoral TLSs in PDAC, both with and without neoadjuvant chemotherapy, using machine-learning image processing platforms.

HOW THIS STUDY MIGHT AFFECT RESEARCH, PRACTICE OR POLICY

⇒ The study proposed that neoadjuvant chemotherapy may compromise the protective roles of intratumoral TLSs, and therefore, should be taken into consideration in the clinical management of PDAC patients receiving presurgery treatment.

INTRODUCTION

Pancreatic ductal adenocarcinoma (PDAC) accounts for more than 90% of all pancreatic cancer cases and has emerged as a global health burden with increasing incidence trends worldwide.[1] Despite significant advances in surgery, chemotherapy and radiotherapy, PDAC prognosis remains disappointing, with a general 5-year survival rate below 10%.[2 3] In addition, immunotherapy against PDAC produces a limited response due to low immunogenicity, high immunosuppression and dense desmoplastic stroma in the PDAC tumor microenvironment (TME).[4] Notably, successful infiltration and activation of T cells in the TME is associated with the exceptional long-term survival in patients.[5] Therefore, further research on strategies to manipulate immune cell infiltration and activation in the PDAC TME is necessary and may hold the key to improving the prognosis of PDAC patients.

Tertiary lymphoid structures (TLSs) are ectopic lymphoid formations developed in

peripheral non-lymphoid tissues including inflamed or cancerous tissues, and they are niches composed of various immune cells (mainly B cells and T cells).[6] Recent studies have revealed that TLSs play important roles in regulating adaptive antitumor immune responses, and the existence of TLSs is closely associated with improved T-cell infiltration and activation.[7 8] Consequently, the presence of TLSs in tumors was proposed as an effective response predictor for patients receiving immune checkpoint inhibitors.[9] The existence and prognostic value of TLSs has been reported in a diversity of cancer types including colorectal cancer,[10] breast cancer,[11] non-small cell lung cancer,[12] gastric cancer[13] and PDAC.[14–16] Tumor-associated TLSs can be located either intratumorally or peritumorally.[17] In PDAC, although TLSs were frequently identified in peritumoral regions, only a small proportion (less than 20%) of PDAC patients had intratumoral TLS structures, and these patients displayed the best prognosis.[14] The results emphasized the significance of intratumoral TLSs in antitumor biology for PDAC patients. Notably, the incidence of intratumoral TLSs in PDAC is much lower than that in other types of solid tumors,[14 17] which hinders the characterization of the spatial organization and cellular composition of PDAC TLSs. In addition, there is still a lack of unified tools based on the presence of intratumoral TLSs for the survival prediction of PDAC patients in clinical application.

Neoadjuvant therapy (NAT) has been widely used as a presurgical treatment for PDAC.[18] Previous studies have reported that NAT can negatively affect TLS development in other cancer types such as breast cancer,[19] metastatic colorectal cancer[20] and lung cancer.[21] Particularly, lung squamous cell carcinoma patients treated with NAT had impaired TLS maturation function compared with the chemotherapy-naïve patients, and the prognostic value of TLS was also lost under the influence of NAT. Notably, this was partly attributed to the immunosuppressive effects of corticosteroids coadministered with chemotherapy.[21] Nevertheless, the role of chemotherapy in antitumor immunity has long been controversial, and how NAT may affect TLS behaviors in PDAC remains largely unknown. A systematic investigation of the characteristics of intratumoral TLSs in PDAC patients with and without NAT is of great significance in understanding the clinical outcomes.

Here, we employed multiplex immunohistochemistry (mIHC) and machine learning image processing software (learned by examples) to analyze PDAC samples from both patients receiving no preoperative treatment and patients receiving neoadjuvant chemotherapy treatment prior to surgery. Intratumoral TLSs from the two groups exhibited different cell compositions and maturation stages and showed differences in immunological characteristics and prognostic relevance. Notably, although the presence of intratumoral TLSs was a beneficial factor for PDAC patients without presurgery treatment, it was not a statistically significant indicator for patients receiving NAT, implying that NAT may exert an important influence on beneficial effects of intratumoral TLSs.

METHODS

Patients and samples

Patients pathologically diagnosed with PDAC were recruited from Shanghai Pancreatic Cancer Institute of Fudan University Shanghai Cancer Center from 2013 to 2019. PDAC tumor tissue specimens (1–2 cm in diameter) were collected from each patient during radical resection surgery and then preserved in the form of formalin-fixed, paraffin-embedded (FFPE) samples for long-term storage.

Before undergoing surgery, the patients were either newly diagnosed without any preoperative cancer-related treatment or had been treated with neoadjuvant chemotherapy under clinical guidelines. These patients were classified into the surgery alone (SA) group (n=380) and NAT group (n=136), respectively, for further study. In the 136 NAT patients, 87 (64.0%) were treated with 2–6 cycles of gemcitabine plus albumin-bound paclitaxel (AG); 22 (16.2%) were treated with 2–8 cycles of gemcitabine plus S-1; 21 (15.4%) were treated with 2–4 cycles of gemcitabine plus oxaliplatin; 5 (3.7%) received 2–4 cycles of folinic acid, fluorouracil, irinotecan plus oxaliplatin; and the other 1 (0.7%) received S-1 alone for two cycles. All the patients in the NAT group, except the one patient treated with S-1 monotherapy, were pretreated with a single 5 mg dexamethasone intravenously prior to chemotherapy to mitigate side effects. Other clinicopathologic features for the two groups, including age, gender, stage (according to the 8th edition of the American Joint Committee on Cancer (AJCC) tumor–node–metastasis (TNM) classification system), T classification, N classification, grade, tumor location, nerve invasion state and vascular invasion state, are listed in online supplemental table S1.

H&E staining

H&E staining was performed on FFPE tissue slides to provide a general picture of PDAC tumor tissues. The cell nucleus was stained with hematoxylin blue, and cytoplasm was stained with eosin pink. Stained tissue specimens were reviewed by two independent pathologists to identify PDAC tumor components.

Fluorescent mIHC

To evaluate the localization and abundance of multiple immune cells in PDAC tissues, fluorescent mIHC was performed in serial sections of FFPE tumor tissue from each PDAC patient using the Opal 7-Colour Manual IHC Kit (PerkinElmer, Hopkinton, Massachusetts, USA) according to the manufacturer's protocol. In each section, 3–5 markers of interest were stained simultaneously using dyes with different fluorescence signals (Opal 520, Opal 570, Opal 620 and Opal 690), and the nuclei were counterstained by DAPI (4′,6-diamidino-2-phenylindole, a blue-emitting fluorescent compound used for nuclear staining). Scanning and analysis of mIHC slides were performed on a Vectra Polaris Automated Quantitative Pathology Imaging System (PerkinElmer, Boston, Massachusetts, USA).

Antibodies for fluorescent mIHC

A total of 23 markers were stained in serial sections of FFPE tumor tissues for each PDAC patient. Common immune cell types including CD4+ T cells (antibody: CD4), CD8+ T cells (antibody: CD8), B cells (antibody: CD20), dendritic cells (antibody: CD11c), regulatory T cells (Treg, antibody: FOXP3), granulocytes (antibody: CD15) and macrophages (antibody: CD68) were first detected to analyze immune cell constitution inside TLSs and immune cell infiltration in the PDAC TME. CD45RO, a marker for active and memory T cells and some B-cell subsets,[22] was also detected. Makers assessing TLS maturation including CD20 (B cells), CD21 (follicular dendritic cells) and CD23 (germinal center B cells). Several T-cell/B-cell activation markers (CD69, CD30, HLA-DR and CD25), costimulation markers (CD28, CD80, CD86, OX40 and OX40L) and inhibitory or exhaustive markers (CTLA-4, PD-1, TIM-3 and LAG-3) were further detected to assess the activation states of TLSs. The sources and epitope retrieval conditions of the antibodies used for fluorescent mIHC in this study are shown in online supplemental table S2.

TLS identification and immune cell quantitation

All mIHC images were captured and analyzed using the software inForm V.2.4 (Akoya Biosciences, Marlborough, Massachusetts, USA), an automated image processing platform based on machine learning, to easily extract information from images of stained tissue sections in single-cell solution. TLSs were recognized as ectopic lymphoid structures with aggregated immune cells (especially B cells and T cells) that lacked integrated organized structures such as capsules. The TLSs were first identified in 10 sections by pathologists and hand drawn as the training regions to train a tissue finder until the training accuracy reached above 97%, and the remaining images were segmented by this automated finder. The original H&E and mIHC staining of each sample would be manually inspected to ensure that the results obtained from the automatic analysis were reasonable.

In this study, we defined the TLS that developed within PDAC tissues in one or more adjacent sections of a sample, as 'intratumoral TLS', while TLS that developed only around the tumor, and/or within the adjacent parenchymal tissue, was defined as 'peritumoral TLS'. Representative images of intratumoral and peritumoral TLS were provided in online supplemental figure S1. Patients with the presence or absence of intratumoral TLSs were classified into TLS (+) and TLS (−) groups, respectively. After that, inForm identified cells using an adaptive algorithmic segmentation, which was also based on machine learning, and assigned phenotypes based on all stained channels. The percentages of positively stained cells inside or outside of the TLS structures were calculated. For samples with more than one intratumoral TLS, the average values for multiple TLSs in the same sample were calculated.

Identification of distinct cell types coexpressing several markers was performed using the Highplex FL module on the HALO V.3.2 image analysis platform (Indica Labs, Albuquerque, New Mexico, USA). Cell segmentation was first performed by nuclear detection and cell membrane and cytoplasm identification. Positivity thresholds for all fluorophores in the mIHC images were then established. Specific cell phenotypes coexpressing different markers were thus automatically identified and quantified in the colocalized markup image.

The densities of tumor-infiltrating immune cells dispersedly distributed around tumor cells or in the tumor stroma were calculated in at least three randomly selected regions for each sample. ImageJ software (Bethesda, Maryland, USA) was also used to help verify the areas of TLSs and the enumeration of immune cells inside and outside TLSs.

Evaluation of prognostic value

Kaplan-Meier survival analysis was conducted to compare the overall survival (OS) and progression-free survival (PFS) probability between PDAC patients with and without intratumoral TLSs. Univariate and multivariate Cox regression analyses were performed to assess whether a parameter was a significant prognostic factor for PDAC. Independent prognostic factors were integrated into a multivariate Cox proportional hazard model to predict the survival of PDAC patients. A user-friendly nomogram integrating several variates of interest was finally established to help estimate the OS probability of PDAC patients. Calibration curves comparing the predictive and actual survival probabilities at 1-year and 3-year time points were drawn to evaluate the predictive performance of the identified model. The predictive value of the nomogram was further verified among another external validation cohort (n=123) randomly enrolled from Fudan University Shanghai Cancer Center. The clinicopathologic information of the external validation cohort is provided in online supplemental table S3.

Statistical analyses

For both the SA and NAT groups, clinicopathologic features were compared between patients with or without intratumoral TLSs using χ^2 test. The OS and PFS probabilities were compared between the TLS (+) and TLS (−) groups using the Kaplan-Meier method. The differences in tumor-infiltrating immune cell densities were compared between TLS (+) and TLS (−) samples by Student's t-test or Mann-Whitney U test depending on data distribution. The areas of TLSs and the percentages of key immune cell types and of cells with positive expression of activation, costimulation or inhibitory molecules among total cells within TLSs were calculated and compared between SA and NAT groups by Student's t-test or Mann-Whitney U test depending on data distribution. All statistical analyses were conducted using SPSS (V.25.0) and R (V.4.1.1) software. Figures were drawn using R (V.4.1.1), Adobe Illustrator (V.26.0.1) and Prism

(V.7.0) software. A two-tailed p value<0.05 was considered to indicate statistical significance.

RESULTS

Identification of intratumoral TLSs in PDAC

To identify TLSs and decipher the cellular composition of PDAC TMEs, we performed fluorescent mIHC analysis of FFPE tumor tissue samples from 380 SA patients and 136 NAT patients. Eight immune cell markers (CD8+ T cells, CD4+ T cells, CD20+ B cells, FOXP3+ Treg cells, CD68+ macrophages, CD15+ granulocytes, CD11c+ dendritic cells and CD45RO+ T/B cells) were costained simultaneously in adjacent sections of PDAC tumor tissues. Multispectral images were processed by the machine learning software inForm and HALO, which can be trained to automatically segment intratumoral TLSs and cells and provide phenotyping results. Representative H&E and fluorescent mIHC images of intratumoral TLSs in the SA and NAT groups of PDAC patients are shown together with the processed images from inForm software and the statistical results (figures 1A–D and 2A–D, online supplemental figure S1). The clinicopathologic characteristics of PDAC patients

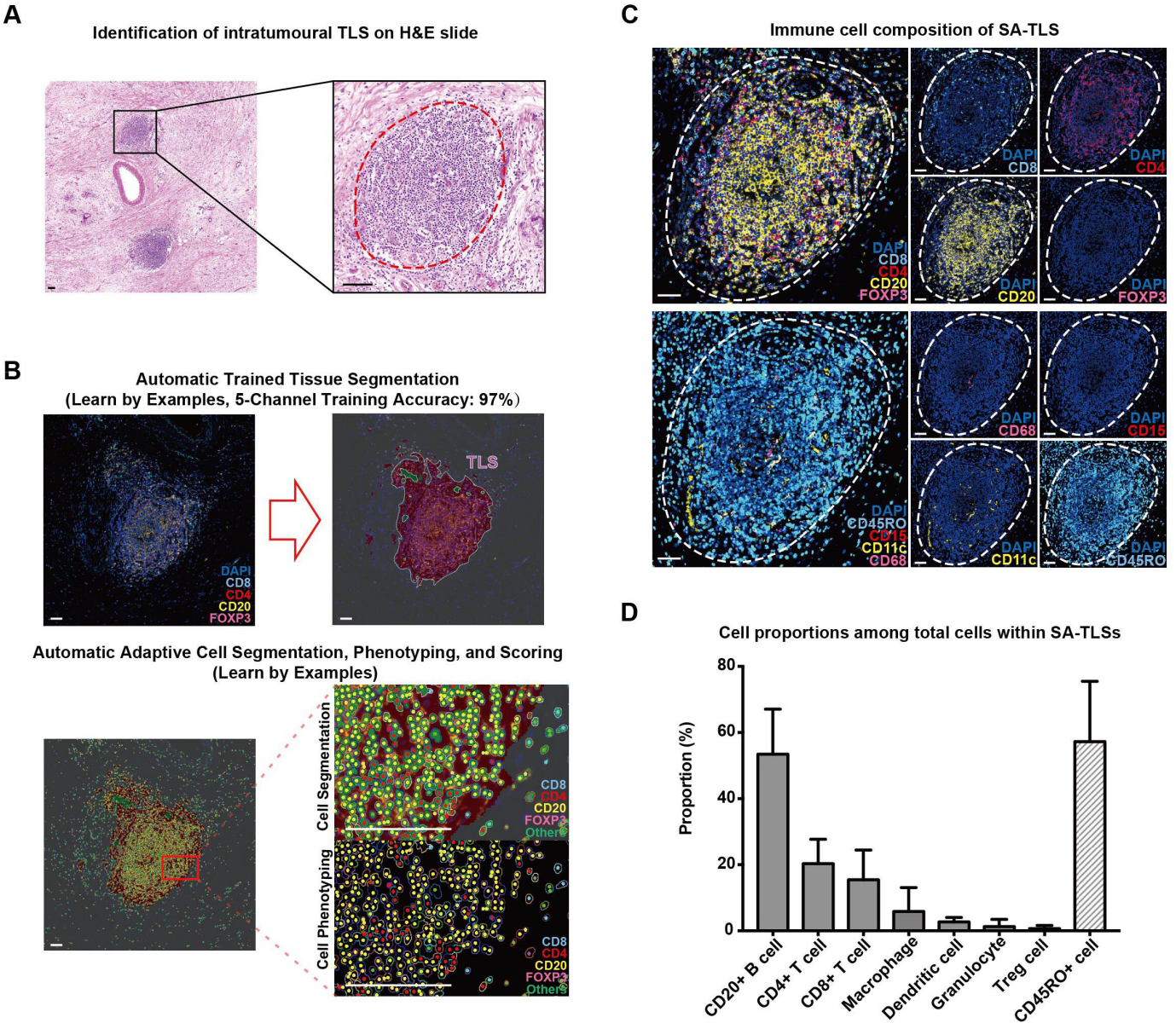

Figure 1 Representative structure of intratumoral tertiary lymphoid structures (TLSs) in surgery alone (SA) patients. (A) H&E staining images of intratumoral TLSs in pancreatic ductal adenocarcinoma tumor tissues; TLS is circled with dotted red line; scale bar: 100 µm. (B) The segmentation of different cell types within TLSs using inForm software; scale bar: 50 µm. (C) Fluorescent multiplex immunohistochemistry staining images combining CD4 (for CD4+ T cells), CD8 (for CD8+ T cells), CD20 (for CD20+ B cells) and FOXP3 (for Treg cells) in one tissue section and CD68 (for macrophages), CD15 (for granulocytes), CD11c (for dendritic cells) and CD45RO in another serial section; TLSs are circled with dotted white lines; scale bar: 50 µm. (D) The proportions of seven immune cells and CD45RO+ cells within intratumoral TLSs in the 80 TLS (+) samples in the SA group.

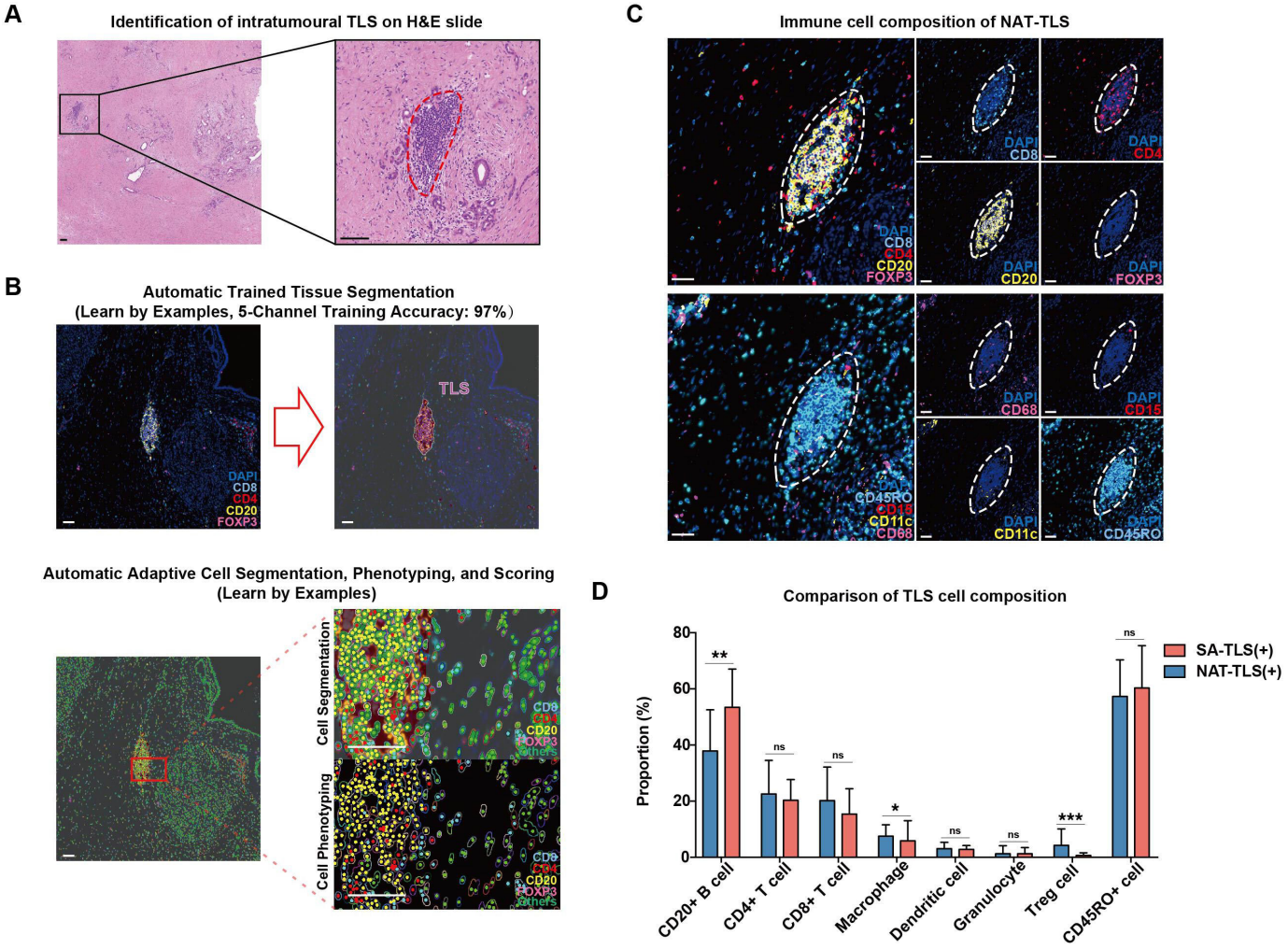

Figure 2 Representative structure of intratumoral tertiary lymphoid structures (TLSs) in neoadjuvant treatment (NAT) patients. (A) H&E staining images of intratumoral TLSs in pancreatic ductal adenocarcinoma tumor tissues; TLS is circled with dotted red line; scale bar: 100 µm. (B) The segmentation of different cell types within TLSs using inForm software; scale bar: 50 µm. (C) Fluorescent mIHC staining images combining CD4 (for CD4+ T cells), CD8 (for CD8+ T cells), CD20 (for CD20+ B cells) and FOXP3 (for Treg cells) in one tissue section and CD68 (for macrophages), CD15 (for granulocytes), CD11c (for dendritic cells) and CD45RO in another serial section; TLSs are circled with dotted white lines; scale bar: 50 µm. (D) Box plots comparing the proportions of seven immune cells and CD45RO+ cells within intratumoral TLSs between the SA (n=80) and NAT (n=21) samples; *p<0.05, **p<0.01, ***p<0.001.

included in this study (online supplemental table S1) and antibodies used for mIHC analysis (online supplemental table S2) are provided in the online supplemental materials.

The clinicopathologic features of TLS (+) and TLS (−) patients in the SA and NAT groups are shown in online supplemental table S4. In the SA group, intratumoral TLSs were identified in 21.1% (80/380) of patients, while in the NAT group, the proportion was reduced to 15.4% (21/136). The TLS (+) proportion of patients receiving AG regimes was even lower, at 13.8% (12/87). The χ^2 test revealed no significant differences in clinicopathologic backgrounds between the TLS (+) and TLS (−) PDAC patients in either the SA or NAT groups (p>0.05, online supplemental table S4).

Cellular composition of intratumoral TLSs in PDAC

The images were further analyzed to quantify the spatial structures and cellular compositions of intratumoral TLSs in the SA and NAT groups. In both SA and NAT groups, TLSs were predominantly composed of CD20+ B cells (53.44% on average for the SA group, 37.88% for the NAT group), CD4+ T cells (20.31% on average for the SA group, 22.57% for the NAT group) and CD8+ T cells (15.42% on average for the SA group, 20.17% for the NAT group) (figures 1C, D and 2C,D). CD20+ B cells were intensively clustered in the central areas of TLSs, while CD4+ T cells and CD8+ T cells were scattered in peripheral T-cell regions (figures 1C and 2C). Small proportions of macrophages and dendritic cells (less than 10%) were identified inside TLSs, and there were fewer granulocytes and Treg cells (less than 5%) in TLSs for both SA and NAT samples (figures 1C,D and 2C,D). In general, the intratumoral TLS structures of the NAT samples had significantly lower proportions of B cells (p<0.01) and higher proportions of Treg cells

(p<0.001) and macrophages compared with SA samples (figure 2D). It should be noted that NAT samples had higher Treg cell proportions within intratumoral TLS than SA samples, but the exact role and function of these Tregs was unknown, since human Tregs display complicated bidirectional feedbacks depending on the immunological context.[23]

CD45RO has been reported to be a marker not only for memory T cells but also for B cells in progressive transition between activation status.[22] In PDAC, remarkable CD45RO expression in both T-cell and B-cell regions of TLSs was also identified in SA (60.29% on average) and NAT (57.32% on average) samples (figures 1C,D and 2C,D).

Association between TLS presence and the levels of tumor-infiltrating immune cells

The densities of tumor-infiltrating immune cells that dispersed surrounding tumor cells or in the stroma, but not within TLSs, were calculated from the digitalized data from inForm and compared between TLS (+) and TLS (−) samples in both SA and NAT groups. Immune cell types with a general mean density greater than 10/mm^2 among all samples were included for analysis.

In the SA group, infiltration levels of CD8+ T cells, CD4+ T cells, CD20+ B cells, CD69+ cells and CD30+ cells in TLS (+) samples were significantly higher than those in TLS (−) counterparts, while the infiltration levels of granulocytes in tumor tissues were lower than those in TLS (−) samples (figure 3A,B and online supplemental figure S2). However, in the NAT group, except CD20+ B cells, no significant differences were observed in infiltration levels of CD8+ T cells, CD4+ T cells and CD69+ cells in TLS (+) samples compared with TLS (−) samples (figure 3C and online supplemental figure S2). Macrophages and CD8+ T cells were the two dominant infiltrating immune cell types in TLS (+) SA samples (figure 3B).

Immune cell infiltration levels were further compared between SA-TLS (+) and NAT-TLS (+) samples and between SA-TLS (−) and NAT-TLS (−) samples. SA-TLS (+) samples had significantly higher infiltration levels of CD8+ T cells, CD20+ B cells and CD69+ cells compared with NAT-TLS (+) samples (figure 3D). In contrast, for SA and NAT samples without intratumoral TLSs, no significant differences were found in CD8+ T cells, B cells and CD69+ cells infiltration levels (figure 3E). Together, the results indicated a significant correlation between intratumoral TLS and immune cell infiltration in SA group, and the administration of NAT also had significant and negative effects on immune infiltration of TLS (+) samples.

Prognostic value of intratumoral TLSs in PDAC

The prognostic significance of intratumoral TLSs was analyzed in both SA and NAT patients. The results of Kaplan-Meier survival analyses indicated that, in the SA group, patients with intratumoral TLSs had significantly better OS (figure 4A) and PFS (figure 4B) than TLS (−) patients. Multivariate Cox regression analyses revealed that the presence of TLSs in tumor tissues was an independent favorable prognostic factor for both OS (HR=0.695, p=0.009) and PFS (HR=0.709, p=0.025) in SA cases (figure 5A). Other independent prognostic factors for the OS of PDAC patients were 8th AJCC TNM stage (HR=1.271, p=0.001) and tumor grade (HR=1.534, p=0.001); TNM stage (HR=1.516, p<0.003) was another prognostic factor for PFS in PDAC patients. However, in the NAT group, the protective effects of intratumoral TLSs on patient OS (p=0.57) or PFS (p=0.81) were not significant in Kaplan-Meier survival analyses (figure 4C,D). Consistently, there were no significant differences in OS or PFS between TLS (+) and TLS (−) patients in any treatment group according to subgroup survival analyses (online supplemental figure S3).

Development and verification of an OS prediction nomogram

To help predict the prognosis of PDAC patients receiving no presurgery drug treatment (SA), we generated a multivariate Cox regression model and a relevant nomogram to predict the survival of PDAC patients.

Three independent prognostic factors for the OS of PDAC (TNM stage, grade and the presence of intratumoral TLS) were included in the multivariate analysis-based nomogram (figure 5B). The survival probability of PDAC patients was predicted based on the equation: logit (P)=0.260×TNM stage+0.430×grade (ref. G1/2)−0.434×TLS classification (ref. TLS (−)). For each patient, survival probability was estimated by weighing the above three prognosis-associated factors.

In the SA group, the calibration curves showed good consistency between the predicted and actual 1-year and 3-year OS rates (figure 5C). To verify the predictive accuracy of the constructed nomogram, we recruited an external validation cohort including 123 PDAC patients who underwent upfront surgery. The presence or absence of intratumoral TLSs in these 123 PDAC patients was quickly determined via H&E staining by pathologists. Patient survival status, follow-up times, ages, tumor stages and grades were also retrieved from Fudan University Shanghai Cancer Center. The OS rates of the external validation cohort were estimated using the nomogram tool and compared with the actual OS rates by calibration curve plotting. The OS prediction capability of the nomogram was satisfactory in the external validation cohort (figure 5D).

Alteration of intratumoral TLS features between SA and NAT groups

As mentioned above, TLS incidence was lower in the NAT group than in the SA group (online supplemental table S4), and intratumoral TLSs in NAT samples had significantly lower B-cell proportions and higher Treg cell and macrophage proportions inside TLS structures compared with the SA group (figure 2D). Moreover, infiltration levels of CD8+ T cells, CD4+ T cells and CD69+ cells in TME were significantly different between NAT and SA groups (figure 3). However, the effects of chemotherapy

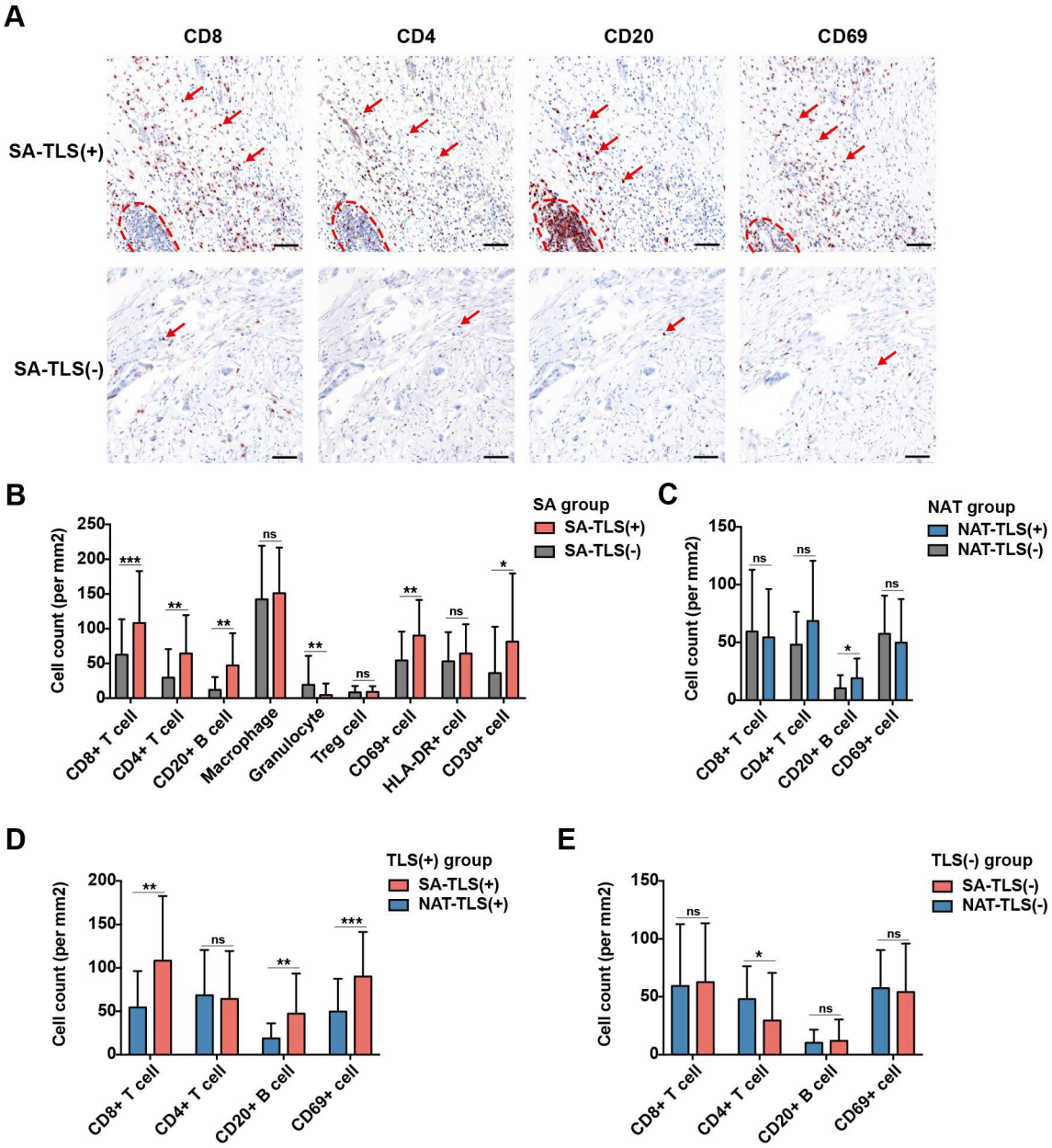

Figure 3 Influence of intratumoral tertiary lymphoid structures (TLSs) on immune cell infiltration in the pancreatic ductal adenocarcinoma tumor microenvironment (TME). (A) Representative brightfield multiplex immunohistochemistry images comparing the infiltration levels of CD8+ T cells, CD4+ T cells, CD20+ B cells and CD69+ cells in TME between TLS (+) samples (n=80) and TLS (–) samples (n=300) in the surgery alone (SA) group; TLSs are circled with dotted red lines; red arrows indicate examples of positively stained cells; scale bar: 100 µm. (B) Boxplots comparing the densities of infiltrated immune cells in TME between TLS (+) samples (n=80) and TLS (–) samples (n=300) in the SA group; *p<0.05, **p<0.01, ***p<0.001, ns: not significant. (C) Boxplots comparing the densities of infiltrated immune cells between TLS (+) samples (n=21) and TLS (–) samples (n=115) in the neoadjuvant treatment (NAT) group. (D) Boxplots comparing the densities of infiltrated immune cells between SA-TLS (+) samples (n=80) and NAT-TLS (+) samples (n=21). (E) Boxplots comparing the densities of infiltrated immune cells between SA-TLS (–) samples (n=300) and NAT-TLS (–) samples (n=115).

on the maturation and functionality of intratumoral TLSs themselves are unclear.

To assess the maturation of intratumoral TLSs, the presence of B cells (marker: CD20), follicular dendritic cells (FDCs, marker: CD21) and germinal center (GC) B cells (marker: CD23) within TLSs were further detected by fluorescent mIHC analysis. TLSs were classified into three maturation stages: early TLS (eTLS, CD20+ CD21– CD23–), primary follicle-like TLS (pTLS, CD20+ D21+ CD23–) with FDC network and secondary follicle-like TLS (sTLS, CD20+ CD21+ CD23+) with germinal center-like structure (figure 6A). Based on the maturation level of TLS, SA and NAT samples were also divided into three categories: eTLS group (sTLS (–) pTLS (–) eTLS (+)), pTLS group (sTLS (–) pTLS (+) eTLS (+/–)) and sTLS group (sTLS (+) pTLS (+/–) eTLS (+/–)). For

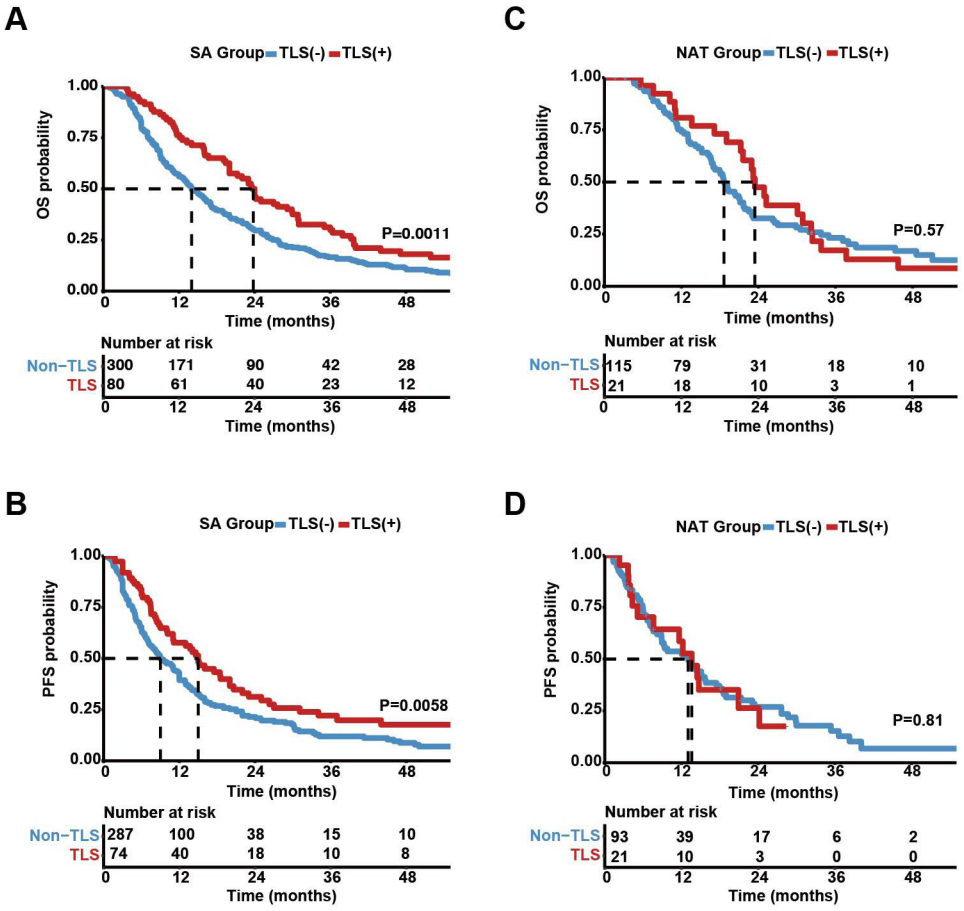

Figure 4 Association between intratumoral tertiary lymphoid structure (TLS) presence and pancreatic ductal adenocarcinoma prognosis. (A,B) Kaplan-Meier curves comparing patient overall survival (OS) and progression-free survival (PFS) probabilities between TLS (+) (n=80) and TLS (–) (n=300) patients in the surgery alone (SA) group. (C,D) Kaplan-Meier curves comparing OS and PFS probabilities between TLS (+) (n=21) and TLS (–) (n=115) patients in the neoadjuvant treatment (NAT) group. Risk tables showing the cumulative numbers of events are provided below.

each TLS (+) sample, especially those with more than one intratumoral TLS at varied maturation stages, the highest TLS maturation stage of all TLSs in a sample was defined as the stage of the sample classification.

PDAC samples with intratumoral sTLS structures had significantly higher levels of CD8+ T-cell infiltration in TME than those with eTLSs (figure 6B), suggesting that the correlation between TLS development and immune cell infiltration was highly dynamic, and that they may influence each other consistently. In addition, we also observed that the sizes of intratumoral TLSs were significantly smaller in the NAT group than in the SA group (figure 6C).

To better evaluate the influence of NAT on TLS maturation, the proportions of samples in the eTLS, pTLS and sTLS groups were compared between SA and NAT cohorts. Among the 80 SA-TLS (+) samples, 63.8% (51/80), 8.8% (7/80) and 27.5% (22/80) were classified as sTLS, pTLS and eTLS group, respectively, whereas in the NAT cohort, the corresponding proportions were 28.6% (6/21), 33.3% (7/21) and 38.1% (8/21), respectively (figure 6D). The proportions of the three subgroups proportions were significantly different between SA and NAT cohorts (p=0.003, χ^2 test), indicating that SA samples may have significantly higher TLS maturation levels than NAT samples.

The association between TLS maturation and prognosis was further analyzed among TLS (+) samples in both SA and NAT groups. For SA patients with intratumoral TLS, the sTLS group turned out to have the best OS (figure 6E), suggesting that different maturation status of intratumoral TLS was correlated with different clinical outcomes for SA patients. However, for NAT patients, neither TLS (+) samples versus TLS (–) samples (figure 4C,D) nor TLS (+) samples with different maturation status (online supplemental figure S5G) had significantly different prognosis, which further demonstrated the impaired prognostic value of intratumoral TLS in NAT-treated PDAC patients.

Characterization of peritumoral TLS features in PDAC

It was suggested that TLS maturation status and location together may display a better prognostic value in certain cancer types.[24] To better decipher the complex association among TLS location, maturation and prognosis in PDAC, we performed further analysis on SA and

A

Univariate and multivariate Cox regression analyses

Covariate	OS				PFS			
	Univariate analysis		Multivariate analysis		Univariate analysis		Multivariate analysis	
	HR(95%CI)	P-value	HR(95%CI)	P-value	HR(95%CI)	P-value	HR(95%CI)	P-value
TLS classification (TLS+ vs. TLS-)	**0.647(0.492,0.851)**	**0.002**	**0.695(0.528,0.915)**	**0.009**	**0.659(0.489,0.889)**	**0.006**	**0.709(0.525,0.958)**	**0.025**
Age (<60 vs. ≥60)	**0.795(0.636,0.993)**	**0.043**	0.858(0.684,1.075)	0.183	1.015(0.802,1.284)	0.902		
Gender (female vs. male)	0.914(0.734,1.138)	0.423			0.905(0.713,1.149)	0.412		
TNM stage (III vs. II vs. I)	**1.365(1.190,1.565)**	**<0.001**	**1.271(1.104,1.463)**	**0.001**	**1.559(1.353,1.795)**	**<0.001**	**1.516(1.309,1.757)**	**<0.001**
T (T3 vs.T1/T2)	**1.530(1.228,1.906)**	**<0.001**			**1.924(1.511,2.450)**	**<0.001**		
N (N1/N2 vs. N0)	**1.706(1.363,2.134)**	**<0.001**			**2.211(1.722,2.838)**	**<0.001**		
Grade (G3 vs. G1/2)	**1.711(1.329,2.203)**	**<0.001**	**1.534(1.186,1.983)**	**0.001**	**1.394(1.100,1.767)**	**0.006**	1.179(0.917,1.517)	0.199
Nerve invasion (yes vs. no)	1.036(0.790,1.358)	0.798			1.182(0.874,1.598)	0.277		
Vascular invasion (yes vs. no)	**1.404(1.085,1.818)**	**0.010**	1.216(0.932,1.586)	0.150	1.600(1.209,2.119)	0.001	1.341(0.999,1.798)	0.050

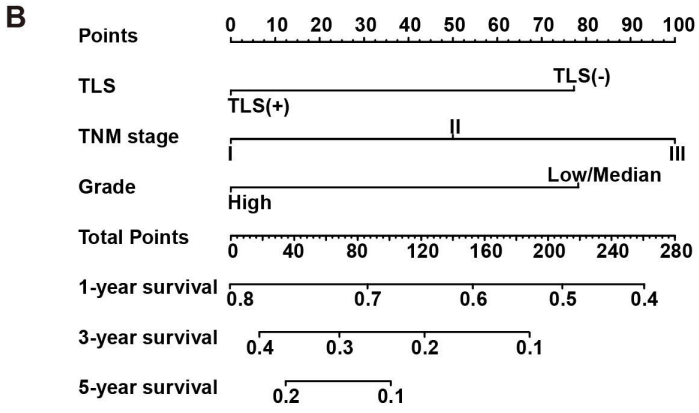

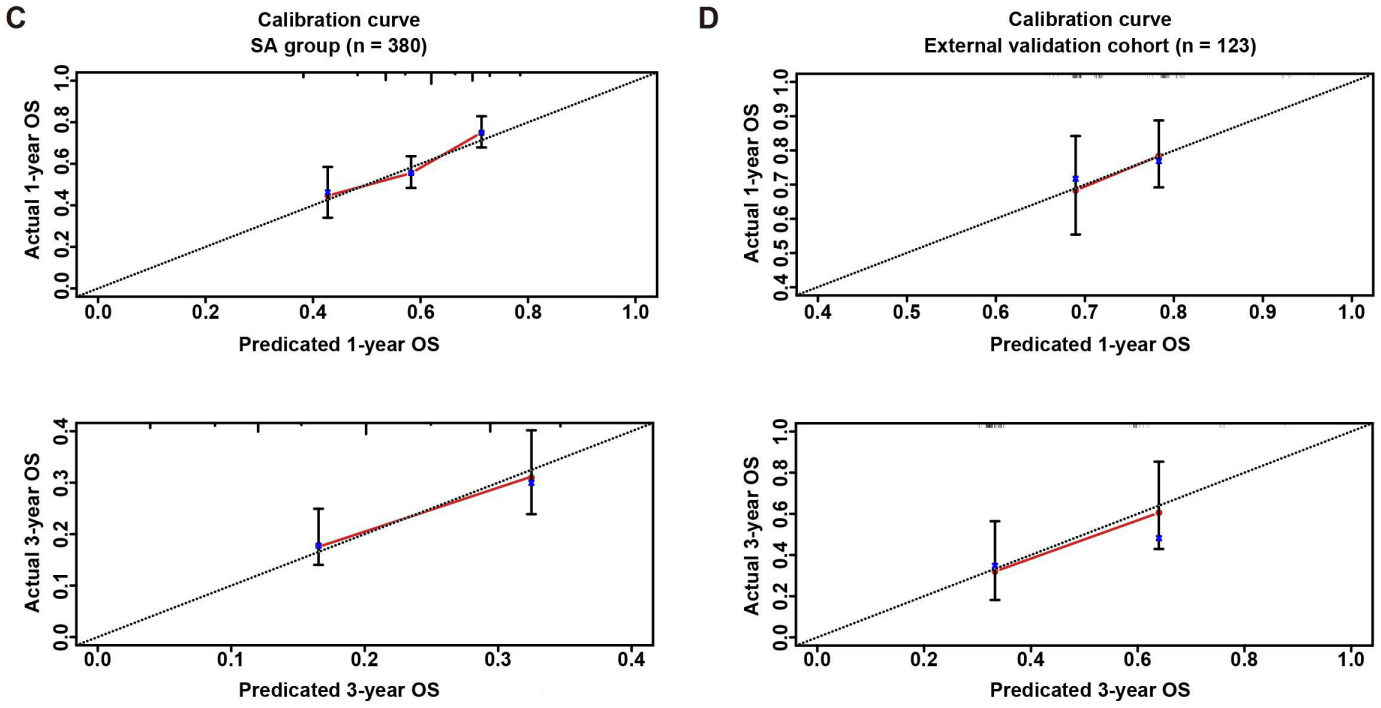

Figure 5 Construction and validation of a nomogram based on multivariate Cox regression analysis. (A) Univariate and multivariate Cox regression analyses for the overall survival (OS) and progression-free survival (PFS) of pancreatic ductal adenocarcinoma (PDAC) patients in the surgery alone (SA) group. (B) The nomogram integrating tertiary lymphoid structure (TLS) presence, tumor–node–metastasis (TNM) stage (American Joint Committee on Cancer 8th edition), and tumor grade for the OS prediction of PDAC patients. (C) Calibration curves for predicting OS at 1-year and 3-year time points in the SA group (n=380); the x-axis indicates the predictive survival probabilities by the nomogram, while the y-axis indicates the actual survival probabilities; the 45° dotted line indicates ideal prediction. (D) Calibration curves for predicting OS at 1-year and 3-year time points in the external validation cohort (n=123).

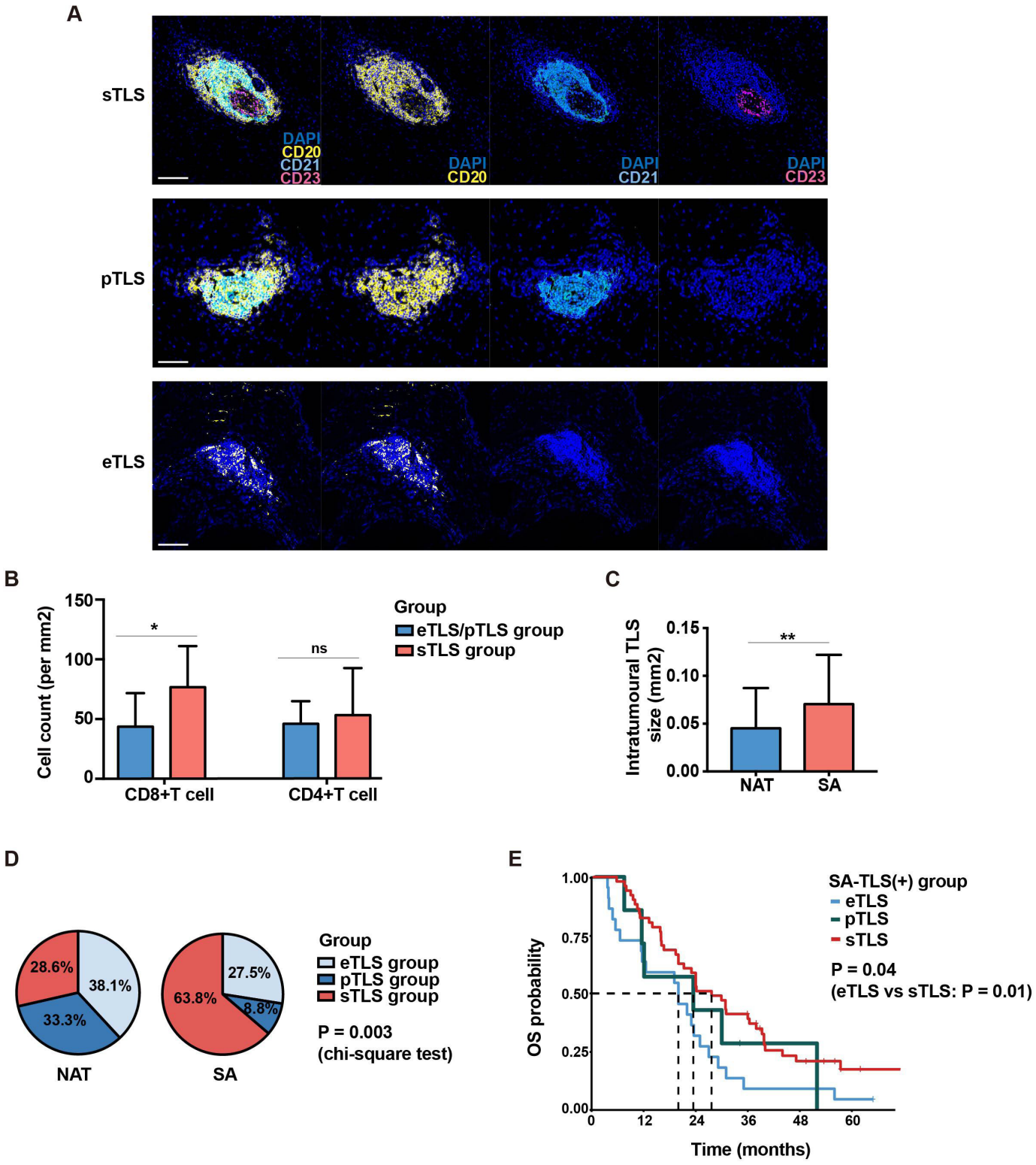

Figure 6 Comparison of tertiary lymphoid structure (TLS) characteristics between the surgery alone (SA) and neoadjuvant treatment (NAT) groups. (A) Representative fluorescent multiplex immunohistochemistry staining images of eTLS (CD20+ CD21− CD23−), pTLS (CD20+ CD21+ CD23−) and sTLS (CD20+ CD21+ CD23+). eTLS, early tertiary lymphoid structure; pTLS, primary follicle-like TLS; sTLS, secondary follicle-like TLS. Scale bar: 100 µm. (B)Boxplots comparing the densities of infiltrated immune cells in tumor microenvironment for all pancreatic ductal adenocarcinoma samples in the sTLS group and eTLS/pTLS groups; *p<0.05, ns: not significant. eTLS group: sTLS (–) pTLS (–) eTLS (+); pTLS group: sTLS (–) pTLS (+) eTLS (+/–); sTLS group: sTLS (+) pTLS (+/–) eTLS (+/–). (C) Comparison of intratumoral TLS sizes between the SA (n=80) and NAT (n=21) group; for samples with more than one intratumoral TLS, the average sizes of TLSs were calculated; **p<0.01. (D) Pie charts comparing the proportions of samples in the eTLS, pTLS and sTLS groups between the SA and NAT cohorts. (E) Survival differences of intratumoral TLS (+) SA samples in the eTLS (n=22), pTLS (n=7) and sTLS (n=51) groups (log-rank test).

NAT samples with analyzable infiltrative tumor borders, followed by characterization of the presence and maturation stages of their peritumoral TLSs.

Of all the analyzed samples, 47.4% (45/95) SA samples (online supplemental figure S4A) and 36.4% (8/22) NAT samples (online supplemental figure S5A) had at least one TLS at a peritumoral location. For SA and NAT cohorts, neither peritumoral TLS presence (online supplemental figure S4B and S5B) nor peritumoral TLS maturation stage (online supplemental figure S4D and S5D) had any significant association with patient survival as intratumoral TLS. To avoid the interference of intratumoral TLSs, intratumoral TLS (−) samples were identified and assessed separately, but the statistical results remained non-significant (online supplemental figure S4C/E and S5C/E).

After that, survival analysis was also performed from the perspective of TLS maturation to investigate whether it was TLS maturation status rather than TLS location that determined the prognostic value of TLS in PDAC. TLS (+) samples with either intratumoral TLS or peritumoral TLS were investigated. As shown in online supplemental figure S4F and S5F, there were no significant survival differences among samples at different TLS maturation stages in both SA and NAT groups. For SA patients, TLS maturation was a prognostic factor in the intratumoral TLS (+) group, but not in the peritumoral TLS (+) group (online supplemental figure S4D/E/G). In contrast, for NAT patients, there was no significant association between TLS maturation and patient prognosis for neither peritumoral TLS (+) (online supplemental figure S5D/E/E) nor intratumoral TLS (+) groups (online supplemental figure S5G).

Overall, these results confirmed the important prognostic value of intratumoral TLS instead of peritumoral TLS for PDAC patients. For SA patients, the presence of intratumoral TLS was a significantly favorable prognostic factor, and high-stage maturation of intratumoral TLS represented a better prognosis; however, the association between peritumoral TLSs and PDAC prognosis was not significant. For NAT patients, neither intratumoral TLSs nor peritumoral TLSs were significantly correlated with patient survival, and TLS maturation status was not a significant prognostic factor either.

Activation of immune cells within intratumoral TLS between the SA and NAT groups

T-cell/B-cell activation, costimulation and inhibitory or exhaustive markers were further analyzed (online supplemental figure S6). For each marker, the percentage of cells with positive staining among the total cells within TLS was calculated. Interestingly, the expression levels of inhibitory markers were rare in most intratumoral TLSs. CD69 and OX40 were frequently observed to be expressed inside TLSs. CD69 is an early activation marker of T cells, and OX40, a TNF-receptor family member, is recognized as a costimulatory factor for T cells and also plays an important role in B-cell development and germinal center formation by interacting with OX40 ligand (OX40L) expressed on B cells.[25]

SA-TLS (+) samples had higher proportions of CD69+ cells and OX40+ cells within TLSs compared with NAT samples (figure 7A). To distinguish the specific immune cell populations expressing these markers, mIHC costaining and colocalization analyses were performed via HALO software. The SA-TLS (+) group turned out to have higher proportions of CD69+ CD4+ T cells, CD69+ CD8+ T cells and OX40L+ CD20+ B cells among total cells within intratumoral TLSs than the NAT-TLS (+) group (figure 7B). The proportions of these activated cell types among their parent populations were also analyzed. Compared with NAT-TLS (+) samples, SA-TLS (+) samples had significantly higher percentages of CD69+ CD4+ T cells and CD69+ CD8+ T cells out of the total CD4+ T cells and CD8+ T cells within TLSs, respectively (figure 7C). The infiltration levels of these activated cell types outside TLSs were also compared between the SA-TLS (+) and NAT-TLS (+) groups. The SA group turned out to have higher infiltration levels of CD69+ CD8+ T cells and OX40L+ CD20+ B cells outside TLSs (figure 7D), and the proportions of CD69+ CD8+ T cells in infiltrating CD8+ T cells were also significantly increased compared with the NAT counterparts (figure 7E). The representative results of the automatic colocalization analysis are provided in figure 7F,G. These results revealed that the SA group had a more activated immune system within intratumoral TLSs compared with the NAT group.

Together, our results provide a comprehensive atlas of intratumoral TLSs with spatial information in the PDAC microenvironment and revealed the effects of NAT on the structure and functionality of TLSs, as summarized in the graphic abstract (figure 8).

DISCUSSION

The presence of intratumoral TLS is a favorable prognostic factor for PDAC patients undergoing upfront surgery

The prognostic value of TLSs has been investigated in many cancers, and the protective effects of TLSs varied, depending on cancer types or certain clinicopathologic parameters, such as tumor stages.[26] In PDAC, TLSs were found to be located at both peritumoral and intratumoral sites, and intratumoral TLSs displayed an important role in antitumor immunology.[14 15 17 27] In this study, we focused on intratumoral TLSs, and investigated their association with the improved clinical outcomes of PDAC patients who underwent upfront surgery (the SA group). We observed that the presence of intratumoral TLSs was not only favorable but also was an independent prognostic factor for both OS and PFS of SA patients, suggesting the possibility of using intratumoral TLSs as a survival prediction tool. Therefore, we generated a comprehensive nomogram combining intratumoral TLS and two other survival-related variables (TNM stage and grade) for the OS prediction of PDAC patients. Compared with a single variable, nomogram represents a major advance in

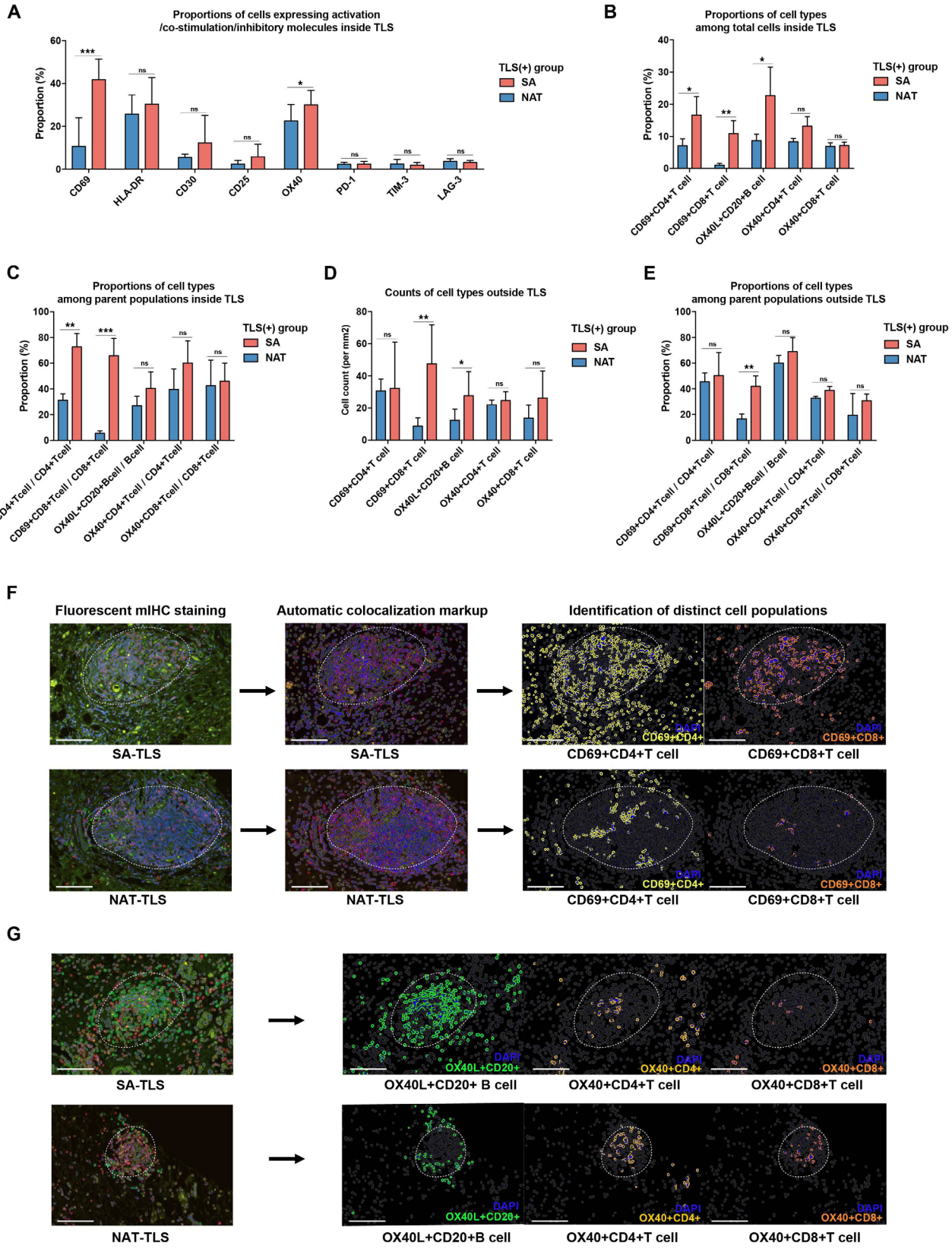

Figure 7 Comparison of activated immune cell populations within or outside intratumoral tertiary lymphoid structures (TLSs) between the surgery alone (SA) and neoadjuvant treatment (NAT) cohorts. (A) Proportions of cells expressing different activation, costimulation and inhibitory markers among all the measured cells within intratumoral TLSs; *p<0.05, **p<0.01, *p<0.05, ***p<0.001. (B) Proportions of activated immune cell types among total cells within TLSs. (C) Proportions of activated immune cell types among parent populations within TLSs. (D) Infiltration levels of activated immune cell types outside TLSs. (E) Proportions of activated immune cell types among parent populations outside TLSs. (F) Representative images for the identification of activated immune cell populations by automatic colocalization analysis; scale bar: 100 µm.

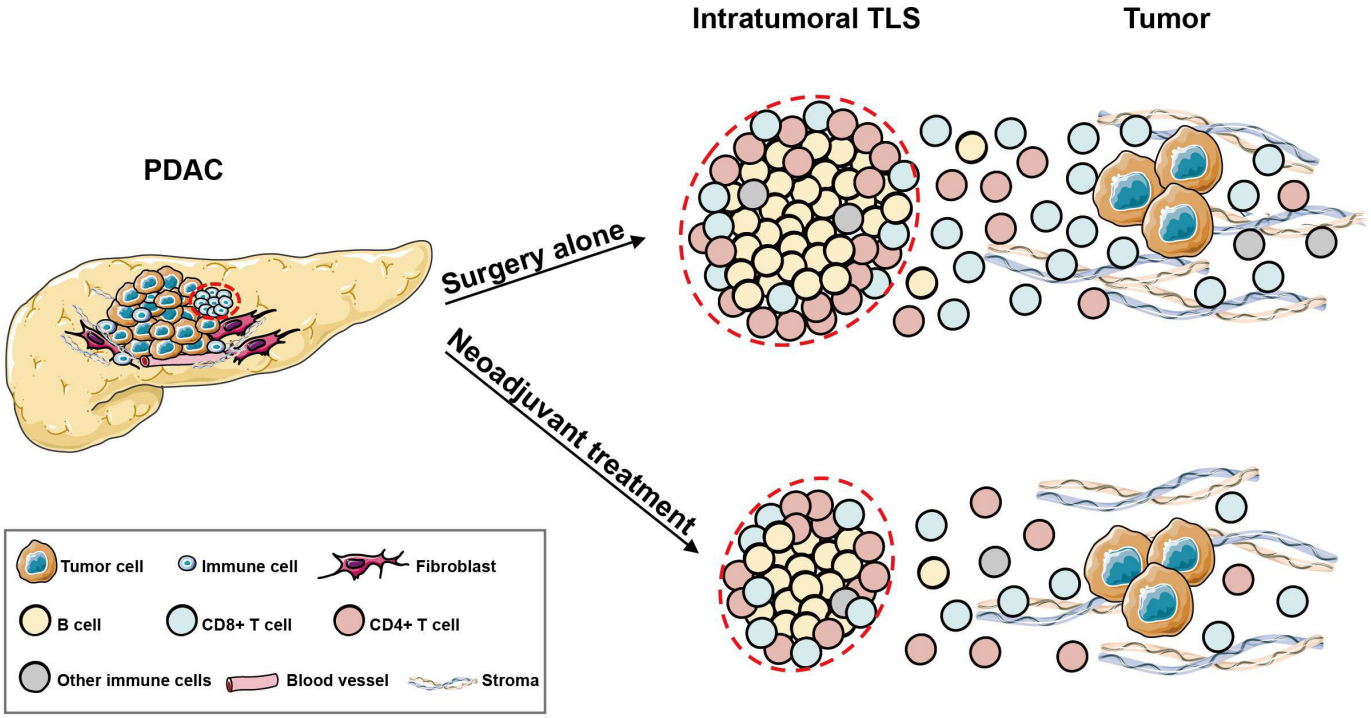

Figure 8 Graphic abstract showing the differences in intratumoral tertiary lymphoid structures (TLSs) between pancreatic ductal adenocarcinoma (PDAC) patients in the surgery alone (SA) and neoadjuvant treatment (NAT) groups. In PDAC, intratumoral TLSs were predominantly composed of CD20+ B cells, CD4+ T cells and CD8+ T cells; the B-cell zone was in the central areas, and the T-cell zone was located in the periphery. Other immune cells, such as macrophages and dendritic cells, only accounted for small proportions. In the NAT group, intratumoral TLSs were smaller in size and inclined to have lower maturation degree. Moreover, the activated immune cell populations inside and outside TLSs were significantly reduced compared with those in the SA counterparts.

precise and individualized risk prediction that may assist in clinical decision-making.[28] In the external validation cohort consisting of 123 PDAC patients, we verified that the constructed nomogram could consistently predict patient OS with a high accuracy.

Intratumoral TLSs in PDAC exhibit unique cellular compositions

Intratumoral TLSs displayed significant heterogeneity in location, cellular composition and spatial organization across different cancers.[17] In the present study, the detailed spatial organization and cellular composition of intratumoral TLSs in PDAC were analyzed by fluorescent mIHC analyses on serial tissue sections. We found that intratumoral TLSs in PDAC typically contained organized B-cell and T-cell zones, with B cells accounting for approximately 50% of all cells, and CD4+ and CD8+ T cells accounting for about 30%–40%. Other less abundant cell types within TLSs included dendritic cells and macrophages that had proportions of less than 10%. In other cancer types, such as lung adenocarcinoma, Treg cells are important components of TLSs that modulate antitumor immune responses.[29 30] However, in PDAC, the presence of FOXP3+ Treg cells within intratumoral TLSs was quite rare. Besides, PDAC TLSs were characterized by abundant CD45RO+ cells in both B-cell and T-cell regions, and both CD45RO+ T cells and B cells contributed to the formation of germinal centers and maturation of TLSs.[16 22 31]

In addition, to better understand the activation status of intratumoral TLSs in PDAC, the expression levels of costimulation (CD28, CD80, CD86 and OX-40) and inhibitory (CTLA-4, PD-1, TIM-3 and LAG-3) markers were further detected. For most samples, we observed high expression of OX-40 within intratumoral TLSs in PDAC. In contrast, the global expression of immune checkpoint molecules was limited. The OX-40/OX-40L axis is an important costimulation signal mediating T-cell–B-cell interaction and may be one of the key regulators of TLS development.[32] Previous studies revealed that increased OX-40 expression was associated with a better prognosis of PDAC patients[33]; anti-OX40 agonists in combination with anti-PD-1 inhibitors may overcome immune escape by repressing the infiltration of Tregs and exhausted T cells in PDAC,[34] suggesting that OX-40 may be a promising therapeutic target for immunotherapies for PDAC, and its exact role in TLS development requires further study.

Does NAT impair the beneficial effects of intratumoral TLSs in PDAC?

There was debate whether all PDAC patients benefit from preoperative NAT,[35] particularly with regard to the establishment of antitumor immunology.[36 37] In this study,

we compared patients receiving NAT and SA to explore the potential influence of NAT on intratumoral TLSs in PDAC. For SA patients, the presence of intratumoral TLSs was closely associated with increased infiltration of various immune cells; however, this phenomenon is not significant in the NAT group, and NAT samples also exhibited a lower proportion of intratumoral TLSs than SA samples, which may impair the normal functions and protective roles of intratumoral TLSs in antitumor immunity for PDAC patients undergoing presurgery treatment.

Previously, NAT was reported to induce neoantigen release and immune activation in PDAC and was therefore beneficial.[36 38] Our data suggested a different perspective that the immune-stimulating function itself of intratumoral TLSs may be impaired after the application of NAT. Generally, the underlying mechanisms of TLS formation harbor both intrinsic and extrinsic factors relevant to tumor cells. On the one hand, neoantigen from cancer cells contribute to the activation of cytokine pathways in relevant to TLS formation (eg, kataegis induced by APOBEC3[39]); on the other hand, different immune cells in the microenvironment may develop self-organization of the TLS,[8] and the administration of chemotherapy may affect both cytokine networking and immune cell behavior, and thus may play both positive and negative roles in the development of TLS.[40] In other words, despite potential immunoenhancement function, poor or non-timely immune recovery after chemotherapy may lead to adverse outcomes.[41 42] For example, chemotherapeutic drug paclitaxel may conversely counteract the expansion of immune cells induced by immune checkpoint blockade.[43] For PDAC patients, the net effects of NAT on the establishment of antitumor immunology may be carefully evaluated.

Besides, corticosteroids that are widely prescribed in clinical practice to impair NAT-related side effects may exert significant immunomodulatory effects on TME.[44] It was reported that the impaired maturation and prognostic value of TLS induced by NAT in lung cancer was partially attributed to the concomitant use of corticosteroids.[21] Similarly, the negative effects of NAT on PDAC-associated TLS development could also be partially attributed to dexamethasone, which should be taken into account in future studies.

In this study, we systematically characterized the cellular properties and prognostic significance of intratumoral TLSs and further explored the potential influence of NAT on TLSs for PDAC patients. The development of TLS is a complex process, and future work may decipher the regulation mechanisms of TLS and attempt to manipulate its antitumor functions to benefit PDAC patients.

CONCLUSION

Overall, this study demonstrated the prognostic value, spatial structure and cellular composition of intratumoral TLSs in PDAC. We found that the presence of intratumoral TLSs promoted antitumor immunity for patients receiving upfront surgery, but NAT may impair the development and maturation of TLS and harm the relevant beneficial effects. For certain PDAC patients, the administration of NAT may require careful consideration in clinical decision-making.

Author affiliations
[1]Department of Pancreatic Surgery, Fudan University Shanghai Cancer Center, Shanghai, China
[2]Department of Oncology, Shanghai Medical College, Shanghai, People's Republic of China
[3]Shanghai Pancreatic Cancer Institute, Shanghai, People's Republic of China
[4]Pancreatic Cancer Institute, Fudan University, Shanghai, People's Republic of China
[5]Department of Pathology Oncology, Fudan University Shanghai Cancer Center, Shanghai, China
[6]Shanghai Key Laboratory of Radiation Oncology, Cancer Research Institute, Fudan University Shanghai Cancer Center, Fudan University, Shanghai, People's Republic of China

Contributors Planning and supervising: XW, CL and XY. Experimenting: XW, XZ, XL, HC and YC. Writing: XZ and XW. Guarantor: XW.

Funding This work was supported by the National Natural Science Foundation of China (grant numbers 82072693, 81902417, 82172884, U21A20374), the Scientific Innovation Project of Shanghai Education Committee (2019-01-07-00-07-E00057), Shanghai Municipal Science and Technology Major Project (21JC1401500), Natural Science Foundation of Shanghai (23ZR1412100), Clinical and Scientific Innovation Project of Shanghai Hospital Development Center (SHDC12018109), Clinical Research Plan of Shanghai Hospital Development Center (SHDC2020CR1006A), National Key Research and Development Program of China (2020YFA0803202, 2022YFC2804800) and Xuhui District Artificial Intelligence Medical Hospital Cooperation Project (2021-011).

Competing interests There is no confilct of interests.

Patient consent for publication Not applicable.

Ethics approval This study involves human participants and was approved by the Ethics Committee of Fudan University Cancer Hospital, ID: 050432-4-2108*. Participants gave informed consent to participate in the study before taking part.

Provenance and peer review Not commissioned; externally peer reviewed.

Data availability statement No data are available.

ORCID iDs
Xianjun Yu http://orcid.org/0000-0002-6697-7143
Xu Wang http://orcid.org/0000-0001-6920-0375

REFERENCES

1 Huang J, Lok V, Ngai CH, *et al*. Worldwide burden of, risk factors for, and trends in Pancreatic cancer. *Gastroenterology* 2021;160:744–54.
2 Siegel RL, Miller KD, Fuchs HE, *et al*. Cancer statistics, 2021. *CA Cancer J Clin* 2021;71:7–33.
3 Tempero MA, Malafa MP, Al-Hawary M, *et al*. Pancreatic adenocarcinoma, version 2.2021, NCCN clinical practice

guidelines in oncology. *J Natl Compr Canc Netw* 2021;19:jnccngls1904:439–57.:.
4 Bear AS, Vonderheide RH, O'Hara MH. Challenges and opportunities for Pancreatic cancer Immunotherapy. *Cancer Cell* 2020;38:788–802.
5 Australian Pancreatic Cancer Genome Initiative, Balachandran VP, Łuksza M, *et al*. Identification of unique Neoantigen qualities in long-term survivors of Pancreatic cancer. *Nature* 2017;551:512–6.
6 Munoz-Erazo L, Rhodes JL, Marion VC, *et al*. Tertiary Lymphoid structures in cancer - considerations for patient prognosis. *Cell Mol Immunol* 2020;17:570–5.
7 Dieu-Nosjean M-C, Goc J, Giraldo NA, *et al*. Tertiary Lymphoid structures in cancer and beyond. *Trends Immunol* 2014;35:571–80.
8 Sautès-Fridman C, Petitprez F, Calderaro J, *et al*. Tertiary Lymphoid structures in the era of cancer Immunotherapy. *Nat Rev Cancer* 2019;19:307–25.
9 Cabrita R, Lauss M, Sanna A, *et al*. Tertiary Lymphoid structures improve Immunotherapy and survival in Melanoma. *Nature* 2020;577:561–5.
10 Trajkovski G, Ognjenovic L, Karadzov Z, *et al*. Tertiary Lymphoid structures in colorectal cancers and their Prognostic value. *Open Access Maced J Med Sci* 2018;6:1824–8.
11 Lee M, Heo S-H, Song IH, *et al*. Presence of tertiary Lymphoid structures determines the level of tumor-infiltrating lymphocytes in primary breast cancer and metastasis. *Mod Pathol* 2019;32:70–80.
12 Rakaee M, Kilvaer TK, Jamaly S, *et al*. Tertiary Lymphoid structure score: a promising approach to refine the TNM staging in Resected non-small cell lung cancer. *Br J Cancer* 2021;124:1680–9.
13 Yin Y-X, Ling Y-H, Wei X-L, *et al*. Impact of mature tertiary Lymphoid structures on prognosis and therapeutic response of Epstein-Barr virus-associated gastric cancer patients. *Front Immunol* 2022;13:973085.
14 Hiraoka N, Ino Y, Yamazaki-Itoh R, *et al*. Intratumoral tertiary Lymphoid organ is a favourable prognosticator in patients with Pancreatic cancer. *Br J Cancer* 2015;112:1782–90.
15 Liudahl SM, Betts CB, Sivagnanam S, *et al*. Leukocyte heterogeneity in Pancreatic Ductal adenocarcinoma: Phenotypic and spatial features associated with clinical outcome. *Cancer Discov* 2021;11:2014–31.
16 Gunderson AJ, Rajamanickam V, Bui C, *et al*. Germinal center reactions in tertiary Lymphoid structures associate with Neoantigen burden, humoral immunity and long-term survivorship in Pancreatic cancer. *OncoImmunology* 2021;10.
17 Rodriguez AB, Engelhard VH. Insights into tumor-associated tertiary Lymphoid structures: novel targets for antitumor immunity and cancer Immunotherapy. *Cancer Immunol Res* 2020;8:1338–45.
18 Neoptolemos JP, Kleeff J, Michl P, *et al*. Therapeutic developments in Pancreatic cancer: current and future perspectives. *Nat Rev Gastroenterol Hepatol* 2018;15:333–48.
19 Acar E, Esendağlı G, Yazıcı O, *et al*. Tumor-infiltrating lymphocytes (TIL), tertiary Lymphoid structures (TLS), and expression of PD-1, TIM-3, LAG-3 on TIL in invasive and in situ Ductal breast Carcinomas and their relationship with Prognostic factors. *Clin Breast Cancer* 2022;22:e901–15.
20 Meshcheryakova A, Tamandl D, Bajna E, *et al*. B cells and ectopic follicular structures: novel players in anti-tumor programming with Prognostic power for patients with metastatic colorectal cancer. *PLoS One* 2014;9:e99008.
21 Siliņa K, Soltermann A, Attar FM, *et al*. Germinal centers determine the Prognostic relevance of tertiary Lymphoid structures and are impaired by corticosteroids in lung squamous cell carcinoma. *Cancer Res* 2018;78:1308–20.
22 Jackson SM, Harp N, Patel D, *et al*. Cd45Ro Enriches for activated, highly Mutated human germinal center B cells. *Blood* 2007;110:3917–25.
23 Rakebrandt N, Littringer K, Joller N. Regulatory T cells: balancing protection versus pathology. *Swiss Med Wkly* 2016;146:w14343.
24 Schumacher TN, Thommen DS. Tertiary Lymphoid structures in cancer. *Science* 2022;375:6576.
25 Fu N, Xie F, Sun Z, *et al*. The Ox40/Ox40L axis regulates T follicular helper cell differentiation: implications for autoimmune diseases. *Front Immunol* 2021;12:670637.
26 Colbeck EJ, Ager A, Gallimore A, *et al*. Tertiary Lymphoid structures in cancer: drivers of antitumor immunity, immunosuppression, or bystander sentinels in disease *Front Immunol* 2017;8:1830.
27 Ding G-Y, Ma J-Q, Yun J-P, *et al*. Distribution and density of tertiary Lymphoid structures predict clinical outcome in Intrahepatic Cholangiocarcinoma. *J Hepatol* 2022;76:608–18.
28 Balachandran VP, Gonen M, Smith JJ, *et al*. Nomograms in oncology: more than meets the eye. *Lancet Oncol* 2015;16:e173–80.
29 Joshi NS, Akama-Garren EH, Lu Y, *et al*. Regulatory T cells in tumor-associated tertiary Lymphoid structures suppress anti-tumor T cell responses. *Immunity* 2015;43:579–90.
30 Devi-Marulkar P, Fastenackels S, Karapentiantz P, *et al*. Regulatory T cells infiltrate the tumor-induced tertiary Lymphoid structures and are associated with poor clinical outcome in NSCLC. *Commun Biol* 2022;5:1416.
31 Kim JR, Lim HW, Kang SG, *et al*. Human Cd57+ germinal center-T cells are the major helpers for GC-B cells and induce class switch Recombination. *BMC Immunol* 2005;6:3.
32 Aspeslagh S, Postel-Vinay S, Rusakiewicz S, *et al*. Rationale for anti-Ox40 cancer Immunotherapy. *Eur J Cancer* 2016;52:50–66.
33 Davis M, Conlon K, Bohac GC, *et al*. Effect of Pemetrexed on innate immune killer cells and adaptive immune T cells in subjects with adenocarcinoma of the Pancreas. *J Immunother* 2012;35:629–40.
34 Ma Y, Li J, Wang H, *et al*. Combination of PD-1 inhibitor and Ox40 agonist induces tumor rejection and immune memory in mouse models of Pancreatic cancer. *Gastroenterology* 2020;159:306–19.
35 Gillen S, Schuster T, Meyer Zum Büschenfelde C, *et al*. Preoperative/Neoadjuvant therapy in Pancreatic cancer: a systematic review and meta-analysis of response and resection percentages. *PLoS Med* 2010;7:e1000267.
36 Mota Reyes C, Teller S, Muckenhuber A, *et al*. Neoadjuvant therapy Remodels the Pancreatic cancer Microenvironment via depletion of Protumorigenic immune cells. *Clin Cancer Res* 2020;26:220–31.
37 Farren MR, Sayegh L, Ware MB, *et al*. Immunologic alterations in the Pancreatic cancer Microenvironment of patients treated with Neoadjuvant chemotherapy and radiotherapy. *JCI Insight* 2020;5:e130362.
38 Kuwabara S, Tsuchikawa T, Nakamura T, *et al*. Prognostic relevance of tertiary Lymphoid organs following Neoadjuvant Chemoradiotherapy in Pancreatic Ductal adenocarcinoma. *Cancer Sci* 2019;110:1853–62.
39 Petljak M, Dananberg A, Chu K, *et al*. Mechanisms of Apobec3 Mutagenesis in human cancer cells. *Nature* 2022;607:799–807.
40 Tran AP, Ali Al-Radhawi M, Kareva I, *et al*. Delicate balances in cancer chemotherapy: modeling immune recruitment and emergence of systemic drug resistance. *Front Immunol* 2020;11:1376.
41 Kang D-H, Weaver MT, Park N-J, *et al*. Significant impairment in immune recovery after cancer treatment. *Nurs Res* 2009;58:105–14.
42 Verma R, Foster RE, Horgan K, *et al*. Lymphocyte depletion and Repopulation after chemotherapy for primary breast cancer. *Breast Cancer Res* 2016;18:10.
43 Zhang Y, Chen H, Mo H, *et al*. Single-cell analyses reveal key immune cell Subsets associated with response to PD-L1 blockade in triple-negative breast cancer. *Cancer Cell* 2021;39:1578–93.
44 Cook AM, McDonnell AM, Lake RA, *et al*. Dexamethasone Co-medication in cancer patients undergoing chemotherapy causes substantial immunomodulatory effects with implications for Chemo-Immunotherapy strategies. *Oncoimmunology* 2016;5:e1066062.